Structural Engineering and Mechanics, *Vol. 65, No. 5 (2018) 547-556*
DOI: https://doi.org/10.12989/sem.2018.65.5.547

Research on damage and identification of mortise-tenon joints stiffness in ancient wooden buildings based on shaking table test

Jianyang Xue*, Fuyu Bai[a], Liangjie Qi, Yan Sui and Chaofeng Zhou

Department of Civil Engineering, Xi'an University of Architecture and Technology, Xi'an 710055, China

(Received April 1, 2017, Revised December 29, 2017, Accepted January 1, 2018)

Abstract. Based on the shaking table tests of a 1:3.52 scale one-bay and one-story ancient wooden structure, a simplified structural mechanics model was established, and the structural state equation and observation equation were deduced. Under the action of seismic waves, the damage rule of initial stiffness and yield stiffness of the joint was obtained. The force hammer percussion test and finite element calculations were carried out, and the structural response was obtained. Considering the 5% noise disturbance in the laboratory environment, the stiffness parameters of the mortise-tenon joint were identified by the partial least squares of singular value decomposition (PLS-SVD) and the Extended Kalman filter (EKF) method. The results show that dynamic and static cohesion method, PLS-SVD, and EKF method can be used to identify the damage degree of structures, and the stiffness of the mortise-tenon joints under strong earthquakes is reduced step by step. Using the proposed model, the identified error of the initial stiffness is about 0.58%-1.28%, and the error of the yield stiffness is about 0.44%-1.21%. This method has high accuracy and good applicability for identifying the initial stiffness and yield stiffness of the joints. The identification method and research results can provide a reference for monitoring and evaluating actual engineering structures.

Keywords: ancient wooden building; mortise-tenon joint; static and dynamic cohesion; stiffness damage; damage identification; shaking table test

1. Introduction

The components in ancient Chinese wooden structures are mainly connected by tenon and mortise joints. The stiffness change of the mortise-tenon joint is nonlinear. The mortise-tenon joint has a good resistance to horizontal thrust, and can effectively reduce the seismic response of the structure (Xue *et al.* 2004). Historically, it is known that mortise-tenon joints become loose and trench damage occurs due to the effect of earthquakes. Thus, the overall structural seismic performance is weakened, and the remaining life of the structures is shortened. To research the stiffness cumulative damage rule and the efficient identification method is of great significance for monitoring and evaluating the health state of ancient wooden structures.

The friction between the column foot and base is isotropic, which shows a clear "ball hinges" nature. In the case of strong earthquakes, the ratio of acceleration response to seismic acceleration of the wooden structures exceeds that of the static friction coefficient. The column foot has great seismic energy dissipation characteristic due to the friction slip, which reduces the damage degree of the upper frame system under the seismic excitation (Yao and Zhao 2006). Column foot slip or lateral displacement of the column can easily cause collapse of the ancient building structure (Zhang *et al.* 2011, Xie *et al.* 2010). The tenon and the mortise have good seismic performance due to friction slip. When strong earthquakes occur, the residual slip of the column feet is larger, the tenon joints and the tenon are pulled out significantly, the bearing capacity of the mortise and the joints decreases, the deformation of the mortise and the connected strata increases, and the structural collapse is more dangerous (Zhao *et al.* 2009). Therefore, it is important to identify the damage parameters of the mortise-tenon joint in advance, which would be helpful for the damage assessment and maintenance of ancient buildings. Xu *et al.* (2012) proposed an improved adaptive weighted iterative algorithm based on the least squares criterion, which had a stable convergency characteristic, high accuracy of the parameters and load identification, and strong noise robustness. Li *et al.* (2016) presented a distributed damage identification approach based on dynamic response under moving vehicle loads, and carried out a damage identification analysis on a simply supported beam with cracks. To address identification problem of frame structures after earthquakes, Chen *et al.* (2014) proposed a new damage identification method based on the wavelet packet decomposition, and pointed out that the damage index could be determined by the change in energy of the structural vibration signal in frequency domain.

Xu *et al.* (2014) analyzed the dynamic responses and damage process of a 15-story steel frame-steel plate shear wall (SPSW) structure. The results indicated that the control platform was numerically stable with fast solution speed and high precision. Xu and Li (2011) presented a theoretical study of a model predictive control (MPC) strategy

*Corresponding author, Ph.D.
E-mail: jianyang_xue@163.com
[a]Ph.D. Candidate
E-mail: baifuyu360@163.com

http://www.techno-press.com/journals/sem&subpage=7
ISSN: 1225-4568 (Print), 1598-6217 (Online)

employed in semi-active control system with magneto-rheological (MR) dampers to reduce the responses of seismically excited structures. Zhang and Xu (2017) proposed a multi-level damage identification method. Numerical studies and laboratory tests were both conducted on a simply supported overhanging steel beam for conceptual vertification. The results demonstrated that the proposed multi-level damage identification via response reconstruction does improve the identification accuracy of damage localization and quantization considerably. Nozari *et al.* (2017) presented an updated linear finite element (FE) model for damage identification of a ten-story reinforced concrete building using ambient vibration measurements. Zhang *et al.* (2017) proposed a novel approach for damage identification of continuum structures based on their dynamic performances. Another damage identification method was proposed by Farahani and Penumadu (2016) for a full-scale, five-girder bridge that sustained sequential damage. The method was based on time-series analysis of vibration data from field measurements and from finite-element (FE) model simulations.

Yang *et al.* (2016) used a fusion sensitivity matrix based on dynamic and static responses to develop a method for damage identification of structures. The relationship between structural stiffness and acceleration response was established by Huang *et al.* (2015), based on the Kalman filter and energy equilibrium theory. By importing the structural energy into the Kalman filter algorithm, the locations of damage and the damage degree were identified. The research results indicate that the modulus under the noise was consistent with the real value. Jayalakshmi and Rao (2017) presented an approach for the identification of system parameters and input dynamic time history. The results show that the algorithm has a good convergence and can be used to identify the non-linear complex structure. He *et al.* (2015) used static and dynamic cohesion and Extended Kalman filter to identify the stiffness and damping damage of the continuous beam. Xu *et al.* (2011) proposed an approximation method for node damage and second-order feature sensitivity. Wang and Yang (2014) studied the different damage states of structural beams and columns by using the vibration response sensitivity damage identification method. Wang *et al.* (2014) carried out wavelet packet decomposition of the acceleration response signals of the nodes on an ancient wood structure beam under random excitation, and proposed the damage index identification of the wavelet packet energy curvature difference. Using this index, the damage identification of an ancient wood structure was carried out.

The methods mentioned above cannot directly identify the stiffness of mortise-tenon joint. In this paper, a shaking table test of an ancient wooden building was carried out at Xi'an University of Architecture and Technology. Based on this test, a simplified mechanical model of the meshing state of the pillar-type ancient wooden structural model was established, and the structural state equation and observation equation were deduced. The relationship between the stiffness of the structure and that of the mortise joint was established by means of the static and dynamic cohesion method. The hammer percussion test and finite element calculations were carried out, and the structural time-history response was obtained. Considering the 5% noise disturbance in the laboratory environment, the stiffness parameters of the mortise-tenon joint were identified by the least squares method and the Extended Kalman Filter method. Using this proposed method, the initial and yield stiffness of the joints can be directly identified with high accuracy.

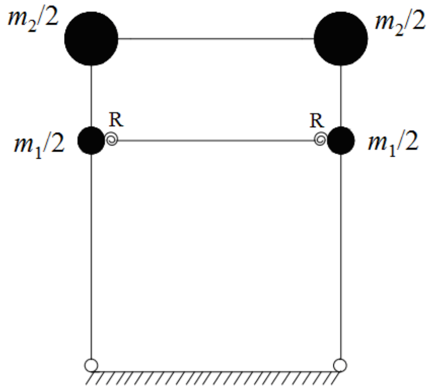

Fig. 1 The simplified mechanical model of wooden structure

2. State and observation equations

2.1 Simplified mechanics model of structure

Ignoring the spatial torsional coupling of structures, a planar simplified model was established according to the experimental model of the ancient building structure, which is shown in Fig. 1. Mortise-tenon joint was simulated by the spring elements, and the beam, column and corbel bracket were modeled by beam element. The structural mass of each region was concentrated on the column top and the bracket layer.

2.2 Structural dynamic equations

$$[M]\{\ddot{\delta}\}+[C]\{\dot{\delta}\}+[K]\{\delta\}=-[M]\{\ddot{\delta}_g\} \tag{1}$$

Where the terms $\{\ddot{\delta}\}$, $\{\dot{\delta}\}$ and $\{\delta\}$ represent the acceleration, velocity and displacement vectors, respectively. $\{\ddot{\delta}_g\}$ is the ground acceleration column vector, $[M]$ is the structural mass matrix, and $[K]$ is the structural stiffness matrix

$$[K]=\begin{bmatrix} k_{11} & k_{12} & k_{13} & k_{14} & k_{15} & k_{16} \\ & k_{22} & k_{23} & k_{24} & k_{25} & k_{26} \\ & & k_{33} & k_{34} & k_{35} & k_{36} \\ & & & k_{44} & k_{45} & k_{46} \\ & \text{symmetry} & & & k_{55} & k_{56} \\ & & & & & k_{66} \end{bmatrix} \tag{2}$$

Damping matrix $[C]=2\zeta\omega^{-1}[K]$, where ζ is the damping ratio, and ω stands for the natural frequency.

The bending elasticity modulus parallel to grain of wood is defined as E, and the moment of inertia of beams, architraves and columns is I_B, I_L and I_C, respectively. The equivalent bending stiffness of the brackets is EI_C. Ignoring the axial deformation of the beam and column, and considering the semi-rigid connections of the rods at both ends, Chopra (2007) has presented the stiffness matrix of the two ends of semi-rigid connecting rods and the hinged ends at one end.

Ignoring the axial deformation, the elastic stiffness matrix of both ends with a rotating spring (semi-rigid connection) unit is

$$[K_{s-s}]=\frac{EI}{L}\begin{bmatrix} k_{01} & k_{03} & -k_{01} & k_{03} \\ & k_{04} & -k_{02} & k_{05} \\ & \text{symmetry} & k_{01} & -k_{03} \\ & & & k_{06} \end{bmatrix} \tag{3}$$

Where

$k_{01}=12(1+2\mu)/(R^*L^2)$; $k_{02}=(6+12\mu)/(R^*L)$;

$k_{03}=(6+12\mu)/(R^*L)$; $k_{04}=(4+12\mu)/R^*$; $k_{05}=2/R^*$;

$k_{06}=(4+12\mu)/R^*$; $R^*=1+8\mu+12\mu^2$; $\mu=EI/(LR)$.

Neglecting the axial deformation, the stiffness matrix of one-hinge-end and one-rigid-end is

$$K_{r-h}=\frac{EI}{L}\begin{bmatrix} \frac{3}{L^2} & \frac{3}{L} & -\frac{3}{L^2} & 0 \\ & 3 & -\frac{3}{L} & 0 \\ & \text{symmetry} & \frac{3}{L^2} & 0 \\ & & & 0 \end{bmatrix} \tag{4}$$

The elements in the stiffness matrix of two different members were assembled, and the structural stiffness matrix and element parameters were obtained.

Assembling the structural stiffness matrix [K], the elements are

$$k_{11}=6EI_C/h_1^3+24EI_D/h_2^3;\ k_{12}=-24EI_D/h_2^3;$$
$$k_{13}=k_{14}=3EI_C/h_1^2+6EI_D/h_2^2;$$
$$k_{15}=k_{16}=6EI_D/h_2^2;\ k_{22}=24EI_D/h_2^3;$$
$$k_{23}=k_{24}=-6EI_D/h_2^2;$$
$$k_{25}=k_{26}=-6EI_D/h_2^2;$$
$$k_{33}=k_{44}=3EI_C/h_1+(4+12\mu)EI_L/(R^*L)+4EI_D/h_2;$$
$$k_{34}=2EI_L/(R^*L);\ k_{35}=2EI_D/h_2;\ k_{36}=0;\ k_{45}=0;$$
$$k_{46}=2EI_D/h_2;\ k_{56}=2EI_B/L;$$
$$k_{55}=k_{66}=4EI_B/L+4EI_D/h_2;$$
$$\mu=EI_L/(RL);$$
$$R^*=1+8\mu+12\mu^2.$$

2.3 Structural state equations and observation equations

Dynamic form

$$\begin{bmatrix} M_{tt} & 0 \\ 0 & 0 \end{bmatrix}\begin{Bmatrix} \ddot{\delta} \\ \ddot{\theta} \end{Bmatrix}+\begin{bmatrix} C_{tt} & C_{ts} \\ C_{st} & C_{ss} \end{bmatrix}\begin{bmatrix} \dot{\delta} \\ \dot{\theta} \end{bmatrix}+\begin{bmatrix} K_{tt} & K_{ts} \\ K_{st} & K_{ss} \end{bmatrix}\begin{bmatrix} \delta \\ \theta \end{bmatrix}=\begin{Bmatrix} -M_{tt}\ddot{\delta}_g \\ 0 \end{Bmatrix} \tag{5}$$

Where $\{\ddot{\theta}\}$, $\{\dot{\theta}\}$ and $\{\theta\}$ are the rotational acceleration, velocity and displacement column vectors, respectively, $[M_{tt}]=\begin{bmatrix} m_{11} & \\ & m_{22} \end{bmatrix}$, K_{tt}、K_{ts}、K_{st}、K_{ss} is the stiffness block matrix. The corresponding block rule is

$$[K_{tt}]=\begin{bmatrix} k_{11} & k_{12} \\ k_{21} & k_{22} \end{bmatrix} \tag{6a}$$

$$[K_{ts}]=[K_{st}]^{-1}=\begin{bmatrix} k_{13} & k_{14} & k_{15} & k_{16} \\ k_{23} & k_{24} & k_{25} & k_{26} \end{bmatrix} \tag{6b}$$

$$[K_{ss}]=\begin{bmatrix} k_{33} & k_{34} & k_{35} & k_{36} \\ k_{43} & k_{44} & k_{45} & k_{46} \\ k_{53} & k_{54} & k_{55} & k_{56} \\ k_{63} & k_{64} & k_{65} & k_{66} \end{bmatrix} \tag{6c}$$

Using the static and dynamic cohesion method to eliminate the zero-mass rotation items, the dynamic equation of the structure is

$$[M_t]\{\ddot{\delta}\}+[C_t]\{\dot{\delta}\}+[K_t]\{\delta\}=-[M_t]\{\ddot{\delta}_g\} \tag{7}$$

The mass matrix of formula (7) is

$$[M_t]=[M_{tt}]=\begin{bmatrix} m_{11} & \\ & m_{22} \end{bmatrix} \tag{8}$$

Stiffness matrix

$$[K_t]=[K_{tt}]-[K_{ts}][K_{ss}]^{-1}[K_{st}]=\begin{bmatrix} K_{11} & K_{12} \\ K_{21} & K_{22} \end{bmatrix} \tag{9}$$

Damping matrix

$$[C_t]=2\zeta\omega^{-1}[K_t] \tag{10}$$

Displacement vector, $\{\delta\}=\{\delta_1 \quad \delta_2\}^T$, where δ_1 and δ_2 are the displacement responses of column layer and bracket layer, respectively.

The above equation of power is transformed into a state equation

$$\frac{d}{d_t}\begin{pmatrix} \delta \\ \dot{\delta} \end{pmatrix}=\begin{bmatrix} 0_x & I_x \\ -[M_t]^{-1}[K_t] & -2\zeta\omega^{-1}[M_t]^{-1}[K_t] \end{bmatrix}\begin{pmatrix} \delta \\ \dot{\delta} \end{pmatrix}+\begin{bmatrix} 0_x \\ -I_x \end{bmatrix}\ddot{\delta}_g \tag{11}$$

Assuming the horizontal speeds of column top and bracket layer were δ_3 and δ_4, and taking the structural stiffness K_{11}, $K_{12}(K_{21})$, K_{22}, damping ratio ζ and the structural first-order natural frequency ω as the five state

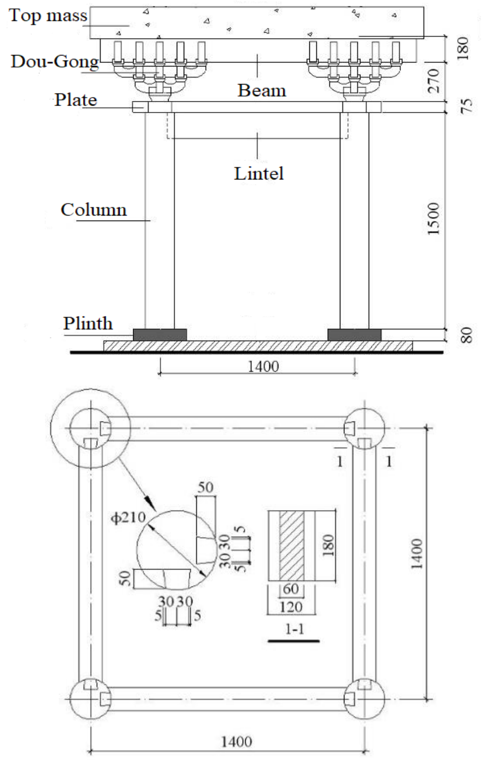

(a) Structural dimensions

(b) Model on the shaking table

Fig. 2 Test model

vectors, the structural state equations are expressed as

$$\begin{cases} \dot{\delta}_1 = f_1 = \delta_3 \\ \dot{\delta}_2 = f_2 = \delta_4 \\ \dot{\delta}_3 = f_3 = -\left(K_{11}\delta_1 + K_{12}\delta_2\right)/m_{11} - 2\zeta\omega^{-1}\left(K_{11}\delta_3 + K_{12}\delta_4\right)/m_{11} - \ddot{\delta}_g \\ \dot{\delta}_4 = f_4 = -\left(K_{21}\delta_1 + K_{22}\delta_2\right)/m_{22} - 2\zeta\omega^{-1}\left(K_{21}\delta_3 + K_{22}\delta_4\right)/m_{22} - \ddot{\delta}_g \\ \dot{\delta}_5 = \dot{\delta}_6 = \dot{\delta}_7 = \dot{\delta}_8 = \dot{\delta}_9 = 0 \end{cases} \tag{12}$$

The structural observation equations are expressed as follows

$$\begin{cases} Z_1 = h_1 = -\left(K_{11}\delta_1 + K_{12}\delta_2\right)/m_{11} - 2\zeta\omega^{-1}\left(K_{11}\delta_3 + K_{12}\delta_4\right)/m_{11} \\ Z_2 = h_2 = -\left(K_{21}\delta_1 + K_{22}\delta_2\right)/m_{22} - 2\zeta\omega^{-1}\left(K_{21}\delta_3 + K_{22}\delta_4\right)/m_{22} \end{cases} \tag{13}$$

3. Parameter identification method

Applying incentives to the bracket layer with weights

$$\begin{cases} K_{11}\delta_1 + K_{12}\delta_2 + 2\zeta\omega^{-1}\left(K_{11}\delta_3 + K_{12}\delta_4\right) = -m_{11}\ddot{\delta}_1 \\ K_{21}\delta_1 + K_{22}\delta_2 + 2\zeta\omega^{-1}\left(K_{21}\delta_3 + K_{22}\delta_4\right) = P_0 - m_{22}\ddot{\delta}_2 \end{cases} \tag{14}$$

When observing the displacement, velocity and acceleration responses of the column top and the bracket layer, the observation matrix X and the stiffness parameter Z are obtained as follows

$$H = \begin{bmatrix} \delta_1 + 2\zeta\omega^{-1}\dot{\delta}_1 & \delta_2 + 2\zeta\omega^{-1}\dot{\delta}_2 & 0 \\ 0 & \delta_1 + 2\zeta\omega^{-1}\dot{\delta}_1 & \delta_2 + 2\zeta\omega^{-1}\dot{\delta}_2 \end{bmatrix} \tag{15}$$

$$X = \begin{bmatrix} K_{11} & K_{12} & K_{22} \end{bmatrix}^T \tag{16}$$

$$Z = \begin{bmatrix} -m_{11}\ddot{\delta}_1 & P_0 - m_{22}\ddot{\delta}_2 \end{bmatrix}^T \tag{17}$$

Based on partial least squares (PLS), structural stiffness parameter $\tilde{X}$ was preliminarily estimated. Considering micro vibration response of the structure, perhaps the calculation process of the coefficient matrix is irreversible. The matrix can be addressed by the signal feature extraction method of singular value decomposition. The noise reflected by the coefficient matrix was separated, and the useful signal was applied in the least squares method (Li and Li 2002).

Extended Kalman filter is a method where the recursive equation of first-order formula is used to estimate the structural damage. This method is suitable for identifying the system parameters of shearing structures. The structure state vector differential equation and the observation equation are shown as follows (Yao *et al.* 2006)

$$\begin{cases} \dot{X} = f(X,t) \\ Y_k = h(X_k, t_k) + \upsilon_k \end{cases} \tag{18}$$

The Extended Kalman filter equations are described below.

State prediction

$$\tilde{X}_k = \hat{X}_k + \int_{t_k}^{t_{k+1}} f\left(\hat{X}_k, t\right) dt \tag{19}$$

Error covariance prediction equation

$$\tilde{P}_{j+1} = \Phi_k P_k \Phi^T{}_k \tag{20}$$

Gain matrix

$$K_{k+1} = \tilde{P}_{k+1} H^T_{k+1} \left(H_{k+1} \tilde{P}_{k+1} H^T_{k+1} + r_{k+1}\right)^{-1} \tag{21}$$

State filtering equation

$$\hat{X}_{k+1} = \tilde{X}_{k+1} + K_{k+1}\left(Y_{k+1} - H_{k+1}\tilde{X}_{k+1}\right) \tag{22}$$

Error covariance filtering equation

$$P_{k+1} = \left(I - K_{k+1}H_{k+1}\right)\tilde{P}_{k+1} \tag{23}$$

Where υ stands for observing noise and r is covariance matrix. The displacement vector, the velocity state vector, the initial error of covariance matrix, the

(a) Joints lateral movement

(b) The pulling out of tenon

Fig. 3 Test phenomenon

column top and the bracket layer acceleration observation vector of the column are known. Then, the extended Kalman filter equation is used repeatedly as the iterative calculation until convergence, and thus, the structural stiffness, damping ratio and other unknown parameters are identified. The state transition matrix of Eq. (20) is shown as follows

$$\Phi_k = e^{A(\hat{X}_k)\Delta t} \approx I + \Delta t \cdot A\left(\hat{X}_k\right) \tag{24}$$

$$A = \left[\frac{\partial f_i\left(\hat{X}_k\right)}{\partial \hat{x}_j}\right] \tag{25}$$

$$H_k = \left[\frac{\partial h_j\left(\hat{X}_k\right)}{\partial \hat{x}_j}\right] \tag{26}$$

Where A is the state Jacobian matrix, H_k is the observed Jacobian matrix, and I is the unit matrix.

4. Seismic damage of mortise-tenon joints

In order to study the cumulative damage of the mortise-tenon joints of ancient wooden structures under the effect of earthquake, a single-layer and single-bay structure with scale of 1:3.52 was tested on the shaking table. The overview of structure model is shown in Fig. 2. As shown in Fig. 2(b), the reinforced concrete slab was loaded with a weight of 14 kN/m^2 as the equivalent roof load, and four pillars were fixed in the 2.0 m × 2.2 m shaking table. A total of 27 data channels were recorded, where 15 channels, 5 channels, and 7 channels were for acceleration measurements, velocity measurements and displacement measurements, respectively. During the loading process, the El Centro waves with different peak accelerations were input. The displacement response, velocity response and acceleration response were obtained. Before and after the earthquake load, a force hammer was used to percuss the structure to produce free vibration.

In the experiment, four seismic waves were selected for the model. Experimental results show that, as the seismic

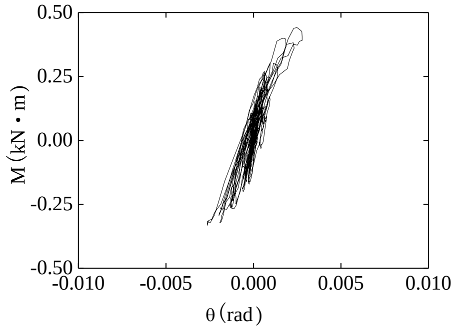

(a) El Centro wave-50 gal

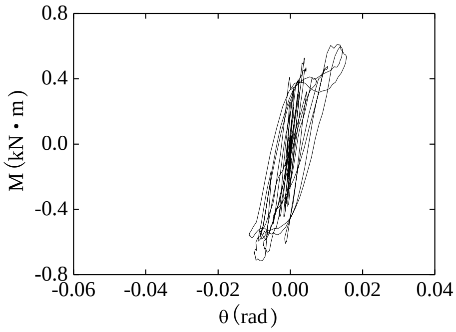

(b) El Centro wave-200 gal

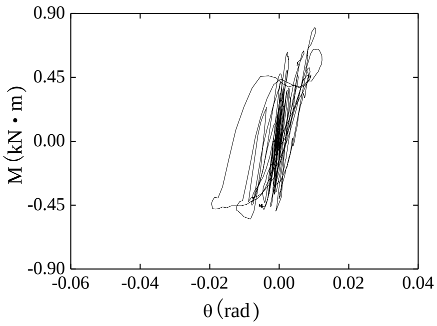

(c) El Centro wave-300 gal

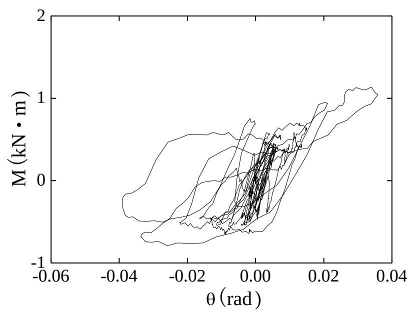

(d) El Centro wave-600 gal

Fig. 4 The moment-rotation curves of the node under different cases

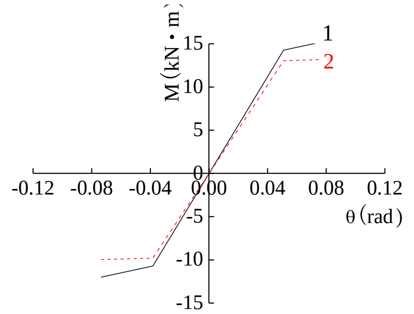

(a) No column feet slip

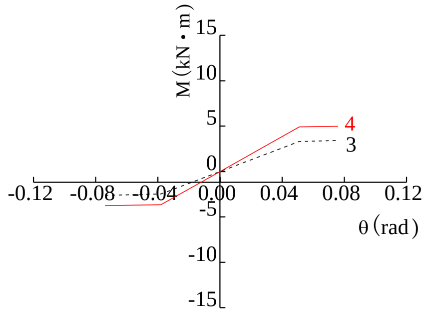

(b) Column feet slip

Fig. 5 The secant stiffness of the node under different cases

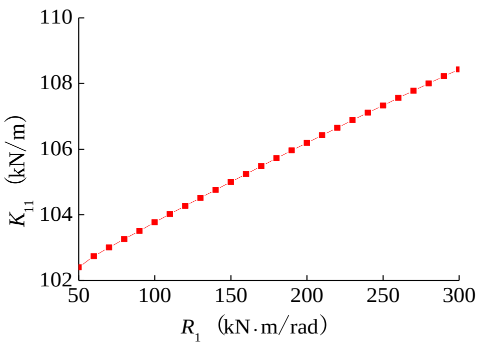

Fig. 6 Relationship between structural layer stiffness K_{11} and node stiffness R_1

loading increases step by step, the displacement of column top and the pulling out degrees of tenon increase, and the structural model collapses when the tenon splits and the column top is broken. When the peak ground acceleration (PGA) of the earthquakes is less than 150 gal, the deformation of the tenon is not obvious. When the earthquakes are excited by PGA of 200 gal, the tenon nodes have less rotation and no trenches. When the input PGA excitation reaches 300 gal, the maximum lateral displacement of column top reaches 28.28 mm and tenon pull out is about 3 mm, as shown in Fig 3. When the input PGA excitation is up to 600 gal, the maximum lateral displacement of column top reaches 56.78 mm and tenon pull out is about 8 mm.

According to the rotation amplitude of the mortise-tenon joints, case 1 is defined as no damage condition, case 2 is the 200 gal earthquake loading, case 3 is the 300 gal earthquake loading, and case 4 is the 600 gal El Centro wave loading. The moment-angle hysteresis curves of the joints are shown in Fig. 4. According to the hysteresis curves, the skeleton curve of the mortise-tenon joints was

Table 1 The secant stiffness values of the node under different conditions

Damage case	Load moment	R_1(kN·m/rad)		R_2(kN·m/rad)	
		True value	Degree of injury	True value	Degree of injury
1	Before loading	279.80	0.00%	36.60	0.00%
2	After 200 gal seismic loading	256.00	8.50%	5.06	86.20%
3	After 300 gal seismic loading	64.88	76.81%	2.90	92.08%
4	After 600 gal seismic loading	96.23	65.61%	4.14	88.69%

Table 2 The ratio of R_1 to R_2

Damage case	1	2	3	4
R_2/R_1	0.131	0.020	0.045	0.043

fitted. For ease of the simulation calculations, the simplified double-line model was used to represent the rotational stiffness of joint in this work. The calculation results are shown in Fig. 5.

As shown in Fig. 5, the stiffness damage of the mortise-tenon joint in case 3 is more aggravated than that of case 1. The initial stiffness in case 3 is only 23.19% of that in case 1, and the yield stiffness in case 3 is only 11.31% of that in case 1. Compared with case 3, the initial stiffness of case 4 increases by 48.32%, and yield stiffness decreases by 29.95%. These results demonstrate that, with the increase in earthquake magnitude, the tenon is pulled out from the mortise of the joint and the force taken by the joint increases. Consequently, the damage degree of the joint yield stiffness increases continuously and the initial stiffness of the node first increases and then decreases.

The mortise-tenon joint rotation stiffness under different cases is shown in Table 1. According to the static and dynamic condensation method, the ancient building structure stiffness parameter K_{11} and tenon joints secant yield stiffness R_1 approach a linear relationship, as shown in Fig 6. For the four cases of K_{11}, real values were 107.99 kN/m, 107.47 kN /m, 102.87 kN /m, and 103.67 kN /m.

Yao *et al.* (2006) carried out a low cyclic reversed load test on the mortise joint model, fitted the restoring force model of the mortise joint, and obtained the proportional stiffness and the yield stiffness of the mortise joint. In this paper, according to the working conditions of the tenon joints of the secant stiffness R_1 and R_2, the yields before and after the line stiffness ratio coefficients are shown in Table 2.

5. Finite element calculation

According to the experimental model, the finite element model was established, as shown in Fig.7. The model column and the number of architraves and beams were simulated with three-dimensional linear two-node unit. Column and the number of mortise connections were simulated with a non-linear rotating spring element. The connection between column feet and base rock was simulated with the assembly unit consisting of axial springs, dampers, gap unit and slider. The brackets were simulated

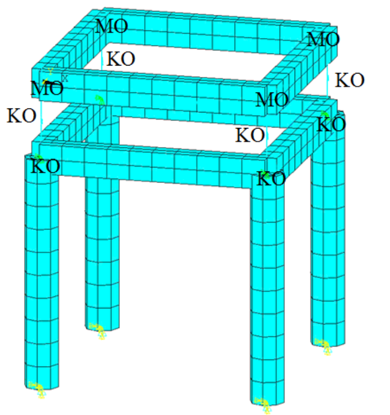

Fig. 7 Finite element model of wooden building

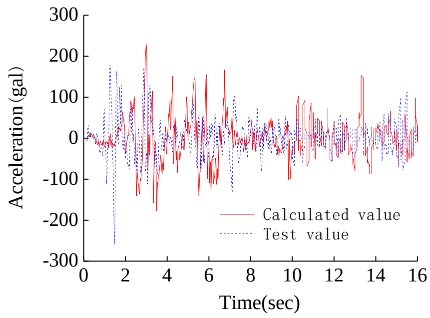

(a) Column feet

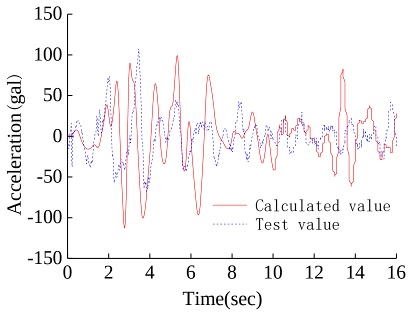

(b) Column top

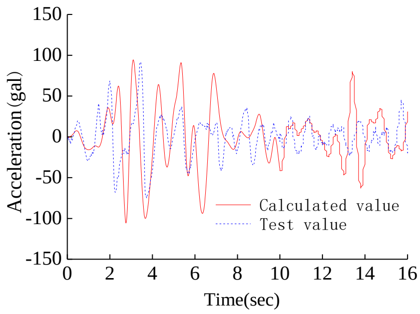

(c) Bracket layer

Fig. 8 The time history curves of acceleration

with horizontal and vertical spring-damper units. The spring unit and the damper were assumed to be of no mass and size. The roof quantity was equivalent to the mass of four nodes which were simulated with 2D unit. The density of the model material was 550 kg/m^3, the flexural modulus of the material was 67.27 MPa, and the stiffness of the mortise-tenon joint was defined by the values mentioned in

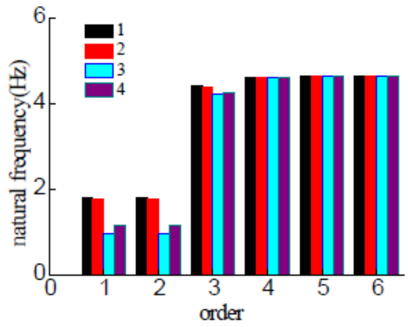

Fig. 9 Natural frequencies of different damage models

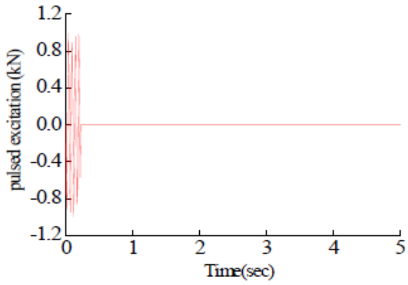

Fig. 10 Pulsed excitation

Table 1. The lateral stiffness and the vertical compressive stiffness of the brackets were determined by the low cyclic loading test and the bearing capacity test (Sui *et al.* 2010, Gao *et al.* 2008). The friction coefficient of the column and the base rock was 0.4.

As shown in Fig. 8, the acceleration time history curves of the column feet, the column and the bracket layer are consistent, and the peak time and size are basically the same. As the peak acceleration increased, especially at 6s-8s and 12s-14s, the joint had a plastic deformation. The friction between the components increased, and the damping ratio of the entire structure became larger. Moreover, the capacity of energy dissipation was enhanced. However, the above-mentioned effect could not be considered in the simulation model, which caused the calculated acceleration to be greater than the experimental acceleration.

The first order natural frequency of finite element analysis in case 1 was 1.88 Hz, and that of the experiment was 2.05 Hz. The relative error of the two calculations was 8.29%. The above analysis shows that the finite element model can meet the requirements of calculation accuracy.

Comparing the first six-order natural frequencies (Fig. 9), it is found that with the increase in damage degree, the first three-order frequencies have an obvious change, and the other order frequencies have no change. The stiffness damage of joint is sensitive to structural low-frequency vibration mode, which indicates that the seismic response of the low frequency can be selected for stiffness identification.

In the shaking table test, the pulsed excitation was produced by hammering a concrete weight on the wood structure. In the process of finite element analysis, the impact of the pulse hammer mass was ignored. As the actual pulsed excitation time was very short, the excitation

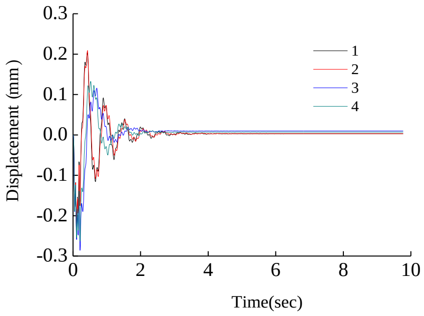

Fig. 11 The time history curves of the column top displacement under different conditions

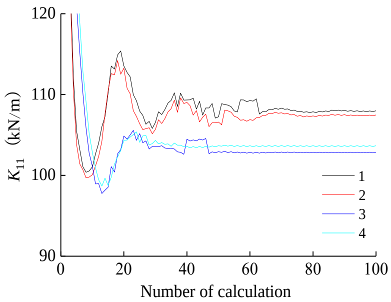

Fig. 12 The convergence curves of K_{11} under different cases with the noise-signal ratio of 0%

time was chosen as 0.2 s. The sampling time of the structural displacement, velocity and acceleration responses was set to 10s and the time step was 0.0098 s. The pulsed excitation is shown in Fig. 10.

Comparing the displacement, velocity and acceleration responses of the column under different damage conditions, it is seen that the maximum negative displsacement of each condition is -0.238 mm, -0.24 mm, -0.286 mm, and -0.263 mm; the corresponding time is 0.107 s, 0.107 s, 0.205 s, and 0.205 s; the maximum positive displacement of each condition is 0.204 mm, 0.209 mm, 0.116 mm, 0.132 mm, and the corresponding time is 0.420 s, 0.430 s, 0.701 s, and 0.520 s, respectively.

Fig. 11 shows that as the stiffness damage of the mortise-tenon joint increases, the negative displacement peak of the joint increases and the positive displacement peak decreases. The negative displacement of the working condition 3 increases by 4.8% and the positive displacement peak decreases by 35.3%. The time when the negative shift reaches peak is delayed by 0.102 s, and the positive displacement peak time is delayed by 0.281 s. To sum up, the displacement and velocity responses for the four kinds of working conditions are basically stable after 4 s.

6. Seismic damage identification

6.1 Structural stiffness parameter approximation identification

The test system of structural response is vulnerable to the influence of observation noise. Considering the test environment with 0% and 5% random noise interference,

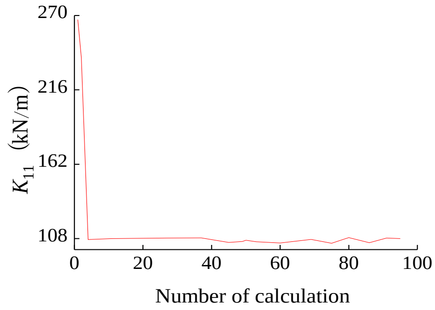

(a) Damage case 1

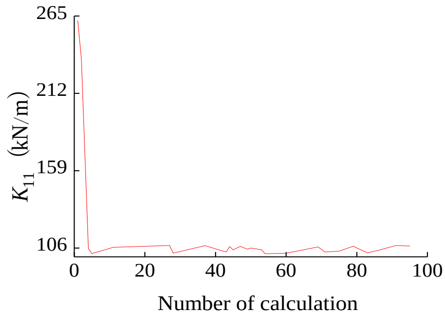

(b) Damage case 2

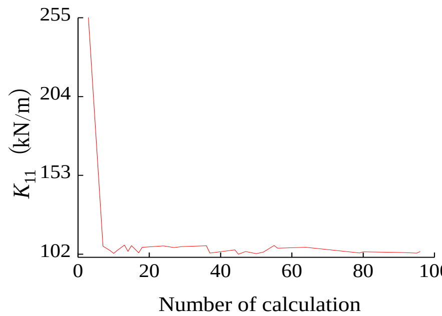

(c) Damage case 3

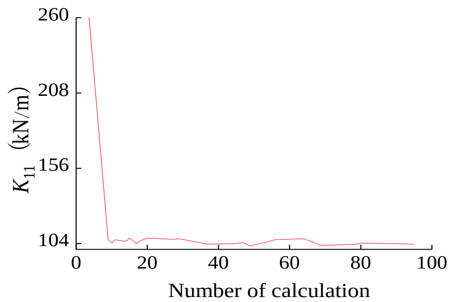

(d) Damage case 4

Fig. 13 The convergence curves of K_{11} under different cases with the noise-signal ratio of 5%

the seismic responses were observed in the simulated noise environment where the Gauss noise was considered.

The observed responses of displacement, velocity and acceleration were used to assemble the observation matrix and the measured vector. The matrix was decomposed by means of the singular value. Under no noise, the convergence curves of K_{11} obtained by the least squares method are shown in Fig. 12.

According to the linear relationship between K_{11} and

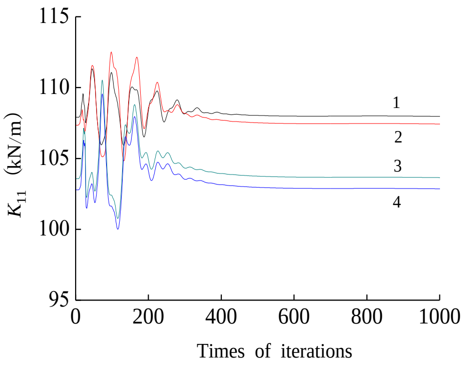

Fig. 14 The convergence curves of K_{11} under different cases

Table 3 Identification values of the EKF parameter

Damage	R_1 Degree of injury	K_{11}(kN/m)	Error (%)
1	0.00%	107.96	-0.03
2	8.50%	107.42	-0.05
3	76.81%	102.85	-0.02
4	65.61%	103.64	-0.03

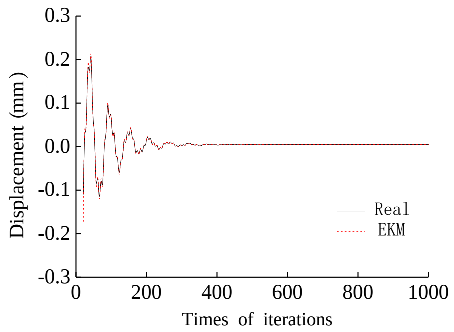

Fig. 15 Comparison between identified value and test value of the column top displacement under 1st loading case

mortise-tenon joint stiffness R_1, the preliminary recognition maximum value of the convergence region K_{11} is 108 kN/m, and the minimum is 102 kN/m.

The curves in Fig.13 represent the efficient stable value of stiffness. As shown in the picture, in the calculation times of 3-100, the relative error statistical values range from -0.5% to 0.5%. Finally, the stiffness value in the 100th time was taken as the initial stiffness value for EKF calculation. Corresponding to the foure cases, the initial stiffness values were 107.91 kN/m, 107.35 kN/m, 102.77 kN/m and 103.57 kN/m, respectively.

6.2 Accurate identification of stiffness parameters of mortise and tenon joints

By using the above parameters as the initial values and adjusting the appropriate covariance, the extended filtering method was used to identify the structural stiffness of K_{11} under various cases, as shown in Fig. 14.

Table 3 shows that under the pulse excitation, the recognition results obtained by extended Calman filter method and least squares method have higher precision, and better stability.

As shown in Fig. 15, the horizontal displacement identification value of the mortise-tenon joint using the EKF method is in good agreement with the real time history trajectory, indicating that the structural stiffness K_{11} is much better.

According to the linear function between K_{11} and R_1, the secant stiffness R_1 can be determined, and then the damage identification value R_2 can be determined according to the ratio of the stiffness before and after the yield, as shown in Table 4.

Table 4 Identification values of the node stiffness

Damage case	R_1(kN·m/rad)	Error (%)	R_2(kN·m/rad)	Error (%)
1	278.18	-0.58	36.44	-0.44
2	253.91	-0.82	5.02	-0.79
3	64.23	-1.00	2.87	-1.03
4	95.00	-1.28	4.09	-1.21

7. Conclusions

Based on the shaking table test of ancient wooden buildings, the cumulative damage rule of mortise-tenon joint was studied. Based on the structural simplified mechanics model, the static and dynamic condensation method was used to establish the relationship between the structural stiffness and mortise-tenon joint stiffness, and the structural state equation and observation equation were deduced. The cumulative damage identification of mortise-tenon joint was studied by means of PLS-SVD and EKF. The main conclusions are summarized as follows:

- With the increase in structural cumulative damage, the damage degree of the joint yield stiffness increases, and the damage degree of the joint initial stiffness first increases and then decreases. The ratios of yield stiffness and initial stiffness are 13.1%, 2.0%, 4.5% and 4.3%, respectively, for the four different damage cases.
- The damage of mortise-tenon joint is sensitive to the low frequency modes of structure. With the increase in structural cumulative damage, the time when the seismic response reaches the peak is advanced. The displacement and velocity peaks of stigma, column feet and bracket layer are larger, and the displacement and velocity responses are basically stable after 4 s.
- The damage identification results of ancient buildings and wood structures show that the hybrid algorithm of static and dynamic condensation, least squares and the Extended Kalman Filter is suitable to quantitatively identify the damage degree of wood structure stiffness.
- The relationship between the initial stiffness of mortise-tenon joint and the stiffness parameters of the structure can be accurately established using the static and dynamic condensation method. Based on the ratio of joint initial stiffness to yield stiffness under different loading conditions, the damage identification of secant stiffness values can be determined under different yield stages. The identified error of the initial stiffness is about 0.58%-1.28%,

and the error of the yield stiffness is about 0.44%-1.21%.

• The pulsed excitation is merely imposed in a certain position of structure, and this method has simple operation, good stability and applicability. The method of obtaining the vibration response by hammering the structure can be applied in the parameter identification of joint stiffness.

Acknowledgments

The authors would like to thank the National Natural Science Foundation of China (Grant No. 51678478), and the Science & Technology Research and Development Program of Shaanxi Province (Grant No. 2013KW23-01) for their generous support of this study.

References

Chen, Q.J., Zhou, C.J. and Yang, Y.S. (2014), "Damage identification of frame structure after earthquakes based on environmental vibration records", *J. Hunan Univ. (Nat. Sci.)*, **41**(9), 20-26.

Chopra, A.K. (2007), *Dynamics of Structures: Theory and Applications to Earthquake Engineering*, 3rd Edition, Pearson Prentice Hall, New Jersey, U.S.A.

Farahani, R.V. and Penumadu, D. (2016), "Damage identification of a full-scale five-girder bridge using time-series analysis of vibration data", *Eng. Struct.*, **115**(5), 129-139.

Gao, D.F., Zhao, H.T. and Xue, J.Y. (2008), *Study on the Structure and Seismic Performance of Chinese Wooden Buildings*, Science Press, Beijing, China.

He, H.X., Lv, Y.W. and Han E.Z. (2015), "Damage detection for continuous girder bridge based on static-dynamic condensation and ekf", *Eng. Mech.*, **32**(7), 156-163.

Huang, X.H., Dyke, S. and Xu, Z.D. (2015), "An in-time damage identification approach based on the Kalman filter and energy equilibrium theory", *J. Zhejiang Univ.-SCI. A (Appl. Phys. Eng.)*, **16**(2), 105-116.

Jayalakshmi, V. and Rao, A.R.M. (2017), "Simultaneous identification of damage and input dynamic force on the structure for structural health monitoring", *Struct. Multidiscipl. Optim.*, 1-28.

Li, G.Q. and Li, J. (2002), *Theory and Application of Dynamic Detection for Engineering Structures*, Science Press, Beijing, China.

Li, H.L., Lu, Z.R. and Liu, J.K. (2016), "Identification of distributed damage in bridges from vehicle-induced dynamic responses", *Adv. Struct. Eng.*, **19**(6), 945-952.

Nozari, A., Behmanesh, I., Yousefianmoghadam, S. and Moaveni, B. (2017), "Andreas stavridis. Effects of variability in ambient vibration data on model updating and damage identification of a 10-story building", *Eng. Struct.*, **151**(11), 540-553.

Sui, Y., Zhao, H.T. and Xue, J.Y. (2010), "Experimental study on lateral stiffness of dougong layer in Chinese historic buildings", *Eng. Mech.*, **27**(3), 74-78.

Wang, J. and Yang, Q.S. (2014), "Numerical Simulation of wood Structure damage identification in", *J. Vibr. Measure. Diagn.*, **34**(1), 160-167.

Wang, X., Hu, W.B. and Meng, Z.B. (2014), "Damage detection of an ancient wood structure based on wavelet packet energy curvature difference", *J. Vibr. Shock*, **33**(7), 153-159.

Wang, X.Y., Huang, W.P. and Li, H.J. (2005), "Inversion of ground motion and identification of structural parametersby ekf", *Engineering Mech.*, **22**(4), 20-23.

Xie, Q.F., Xue, J.Y. and Zhao, H.T. (2010), "Seismic damage investigation and analysis of ancient buildings in Wenchuan earthquake", *J. Build. Struct.*, **31**(2), 18-23.

Xu, B. and He, J. (2012), "Structural parameters and dynamic loading identification with partially unknown excitations", *Chin. Civil Eng. J.*, **45**(6), 13-22.

Xu, L.H., Li, Z.X. and Lv, Y. (2014), "Nonlinear seismic damage control of steel frame-steel plate shear wall structures using MR dampers", *Earthq. Struct.*, **7**(6), 937-953.

Xu, L.H. and Li, Z.X. (2011), "Model predictive control strategies for protection of structures during earthquakes", *Struct. Eng. Mech.*, **40**(2), 233-243.

Xu, L.H., Li, Z.X. and Qian, J.R. (2011), "Test ananlysis of detection of damage to a complicated spatial model structure", *Acta Mech. Sin.*, **27**(3), 399-405.

Xue, J.Y., Zhao, H.T. and Zhang, P.C. (2004), "Study on the seismic behaviors of Chinese ancient woodn buolding by shaking table test", *Chin. Civil Eng. J.*, **37**(6), 6-11.

Yang, C., Hou, X.B., Wang, L. and Zhang, X.H. (2016), "Applications of different criteria in structural damage identification based on natural frequency and static displacement", *SCI. CHIN. (Technol. Sci.)*, **5**(11), 1746-1758

Yao, K. and Zhao, H.T. (2006), "Study on the mechanism of sliding friction shock isolation between timber column and plinth in historical", *Eng. Mech.*, **23**(8), 127-131.

Yao, K., Zhao, H.T. and Ge, H.P. (2006), "Experimental studies on the characteristic of mortise-tenon joint in historic timber buildings", *Eng. Mech.*, **23**(10), 168-173.

Zhang, C.D. and Xu, Y.L. (2017), "Multi-level damage identification with response reconstruction", *Mech. Syst. Sign. Proc.*, **95**(10), 42-57.

Zhang, W.S., Du, Z.L., Sun, G. and Xu, G. (2017), "A level set approach for damage identification of continuum structures based on dynamic responses", *J. Sound Vibr.*, **386**(1), 100-115.

Zhang, X.C., Xue, J.Y. and Zhao, H.T. (2011), "Experimental study on Chinese ancient timber-frame building by shaking table test", *Struct. Eng. Mech.*, **40**(4), 453-457.

Zhao, H.T., Zhang, H.Y. and Xue, J.Y. (2009), "Stiffness analysis of dovetail joints of ancient architecture wood structures", *J. Xi'an Univ. Architect. Technol.*, **41**(4), 450-451.

CC